Springer

KSME

Journal of Mechanical Science and Technology 25 (9) (2011) 2185~2193
www.springerlink.com/content/1738-494x
DOI 10.1007/s12206-011-0529-2

Effect of microstructure and chemical composition on cold crack susceptibility of high-strength weld metal †

Hui-Jun Yi*, Yong-Jun Lee, Jong-Yun Kim and Sung-Su Kang

School of Mechanical Engineering, Pusan National University, Busan, 609-735, Korea

(Manuscript Received January 12, 2011; Revised April 4, 2011; Accepted May 2, 2011)

Abstract

The effects of the microstructural constituents, chemical composition, and retained austenite on high-strength weld metal were studied using preheat-free steels and GMAW solid wires with a low hydrogen content. The cold cracking susceptibility of these GMAW wires was evaluated using the y-groove Tekken test. The results showed that acicular ferrite produced the greatest resistance to cold cracking and that the microstructure of the deposit was more important than the hardness and diffusible hydrogen content in low-hydrogen weld metal. Crack blunting and branching occurred when a crack propagated through fine acicular ferrite because of the fine interlocking nature of the microstructure. Alloying elements for nucleating acicular ferrite, such as Ti, Al, and V, are required for proper austenite grain size, and sequence of inclusion formation was identified in the present paper. Furthermore, the retained austenite was not found to play the role of a hydrogen trapping site and so had no effect on the cold cracking susceptibility at a low preheating temperature (≤100℃) and low heat input (≤1.5 KJ/mm) to the weld metal.

Keywords: Weld metal; Cold crack; Acicular ferrite; Grain size; Retained austenite

1. Introduction

Cold cracking, or hydrogen-induced cracking, generally occurs at temperatures below 200℃. It is also called "delayed cracking" due to the incubation time required for crack development. It is generally accepted that cold cracking will occur when the following factors are present simultaneously: diffusible hydrogen in the weld metal, a susceptible microstructure, and residual stress [1].

In the past, cold cracking was most commonly observed in the heat affected zone (HAZ) of high-strength steels, and for avoiding the cold cracking, some have proposed the use of a carbon equivalent as a steel weldability indicator, with the principal aim being the determination of the minimum necessary preheating temperature for welding high-strength structural steels, because the most reliable and fail-safe measure to avoid cold cracking is preheating [2]. The concept of most carbon equivalents is that the higher hardness value of the HAZ is more susceptible to cold cracking and that preheating is able to allow a low cooling rate to obtain a lower hardness value for the HAZ [2, 3]. This can be also avoided in the new generation of high-strength steels with improved weldability, such as thermo mechanical controlled process (TMCP) and high-performance steels (HPS), by lowering the proportion of alloying elements [4, 5]. These steels maintain a less-susceptible microstructure in their HAZ and are often called "preheat-free steels" [6]. However, the welds themselves are now more prone to cold cracking than the HAZ of the base metal in such high-strength steels. In particular, weld-metal cold cracking has been reported to be a major limiting factor in the use of TMCP and high-performance steels without preheating. The known principal factors influencing cold cracking in weld metal are the strength of the weld metal, hydrogen level, microstructure, restraint, and weld cooling rate.

The first purpose of the present study was to find a microstructural constituent that would improve cold cracking resistance. We confirmed that the acicular ferrite which is known as microstructure improves the toughness of the weld metal, and the resistance to cold cracking was the most dominant microstructure that could prevent cold cracking in the weld metal.

TiO, TiN, Al_2O_3, and VN promote the formation of acicular ferrite, acting as point sites from which intragranular nucleation is developed [7-9]. It is known that austenite grain size has a very profound effect on the nucleation rate of acicular ferrite and that acicular ferrite formed from large austenite grains tends to be fine, while acicular ferrite formed from small austenite grains tends to be relatively coarse [10]. Thus,

† This paper was recommended for publication in revised form by Associate Editor Vikas Tomar

* Corresponding author. Tel.: +82 10 4846 3184, Fax.: +82 55 269 2303
E-mail address: yi.h.jun@gmail.com

Table 1. Chemical and mechanical properties of base metal.

	C	Si	Mn	Ni	Cr	Mo	Cu	Al	Nb	B	T.S (MPa)	Y.S (MPa)	EI (%)	Pcm
Base metal	0.09	0.07	1.71	0.007	0.05	0.03	0.01	0.048	0.025	0.0002	614.0	733.0	21.0	0.182

Table 2. Chemical compositions and diffusible hydrogen content of weld metal.

Identification		C	Si	Mn	Ni	Cr	Mo	Al	Ti	V	Pcm	HD (㎖/100g)
ER100S-G	WA100	0.057	0.340	1.081	1.275	0.284	0.219	0.006	0.006	0.08	0.193	1.15
	WB100	0.095	0.382	0.871	0.504	0.456	0.193	0.005	0.006	0.001	0.197	1.48
	WC100	0.053	0.306	0.987	1.262	0.266	0.197	0.005	0.006	0.08	0.174	1.43
ER110S-G	WD110	0.070	0.592	1.285	1.730	0.304	0.539	0.006	0.006	0.002	0.250	1.68
	WE110	0.091	0.510	1.312	1.618	0.269	0.452	0.016	0.006	0.002	0.269	1.33
ER120S-G	WF120	0.086	0.590	1.382	1.946	0.290	0.516	0.016	0.032	0.003	0.269	1.08

Table 3. Results of mechanical tests performed on all weld metal specimens.

Identification	Yield strength (MPa)	Tensile strength (MPa)	Elongation (%)	Charpy impact toughness (J)			
				-10℃	-30℃	-50℃	-70℃
WA100	639.0	702.7	22.0	48.3	37.6	33.3	13.7
WB100	502.7	579.2	22.0	104.5	73.2	37.9	29.7
WC100	599.8	662.5	22.0	76.8	53.6	39.2	17.3
WD110	778.6	838.4	20.0	97.7	81.4	63.4	46.1
WE110	838.4	878.1	19.0	79.0	71.2	62.7	48.3
WF120	847.9	970.8	20.0	60.4	52.6	38.2	30.7

the second purpose of this study was to determine the influence of the chemical composition and austenite grain size on the formation of the microstructure. The weld composition and austenite grain size must have had the effect of promoting the acicular ferrite transformation. If these conditions are not met, the austenite will transform into bainite or coarse ferrite, depending on the cooling rate [7]. We suggested that the sequence of inclusion formation in Al-V-Ti-Si-Mn deoxidized steel weld metals might be outlined as follows and confirmed that the austenite grain size is important in determining the proportions of the acicular ferrite transformation from the test results. It is also concluded that enough austenite grain size and retention time are needed for nucleating the acicular ferrite.

The third purpose of the present study was to determine the influence of retained austenite and observe crack propagation and the fracture modes in high-strength weld metal. The effect of the retained austenite on the cold cracking susceptibility has been researched, and it has been reported that the retained austenite in high-strength steel welds is a strong hydrogen trapping site that must be considered in the determination of hydrogen cracking susceptibility [11]. Moreover, once diffusible hydrogen saturation has been achieved, it has been suggested that further increases in the presence of this phase may only be beneficial at lower diffusible hydrogen concentrations. Furthermore, it was reported that increases in the presence of second phase austenite were beneficial due to the impediment of crack growth by the interface [12]. But, in this study, we concluded that retained austenite had no effect on the cold cracking susceptibility because no retained austenite was found in the weld metal with a low preheating temperature ($\leq$ 100℃) and low heat input ($\leq$ 1.5 KJ/㎜).

Cold cracks developed mainly in an intragranular fracture mode along the columnar grain boundaries and small micro cracks could be situated in either grain boundary ferrite or intragranular microstructures.

2. Experimental procedure

2.1 Base metal and welding consumables

The mechanical and chemical properties of the preheat-free base metal are given in Table 1. The chemical composition of the welding consumables analyzed in weld deposits where 80% Ar + 20% CO_2 gas shielding was used and reported in Table 2. The diffusible hydrogen content of each weld metal was measured by the gas chromatograph method following the AWS specification [13] and is also given in Table 2. The mechanical properties of each weld metal are recorded in Table 3. Test specimens for mechanical tests of base metal and weld metal were prepared and conducted according to ASTM A 370 [14] and AWS D 1.1 [15]. The chemical compositions were obtained by the spectrochemical analysis.

Table 4. Y-groove Tekken test welding parameters.

Identification	Current (A)	Voltage (V)	Speed (cm/min)	Heat input (KJ/mm)
WA100	278.0	28.8	40.0	1.20
WB100	270.0	28.8	40.0	1.17
WC100	278.0	28.8	40.0	1.20
WD110	264.0	28.8	40.0	1.14
WE110	260.0	28.8	40.0	1.12
WF120	270.0	28.8	40.0	1.17

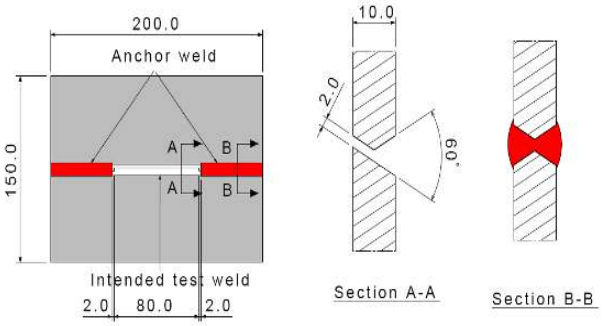

Fig. 1. Schematic illustration of the Y-groove Tekken test principle.

2.2 Y-groove Tekken test

To study the cold cracking of the weld metal, the relatively simple and widely used y-groove Tekken test was adopted in the present study. Y-groove Tekken test specimens were prepared as shown in Fig. 1. Table 4 shows the welding conditions for test weld beads that were applied in the fabrication site. Three different preheating temperatures (15℃, 35℃, and 75℃) were selected.

2.3 Microstructural analysis and hardness test

The weld metal microstructures of each specimen were characterized using optical microscopy. A 2% nital solution was used as the enchant and more than 20 micrographs were taken at ×500 magnification and analyzed according to the IIW recommendation [16]. The hardness was measured by the macro-Vickers hardness test, per ASTM E92-82 (2003), with a load of 5 kg and 10 s of loading time. Measurements were made 2 mm from the top of the weld metal.

2.4 Cracking propagation and failure analysis

An optical microscope and a Jeol JSM-5610 scanning electron microscope (SEM) were used for fractographical observations. To determine the probable crack propagation paths, cross sections of the cracked specimens were first observed with the microscope and then intentionally fractured by a tensile and bending test apparatus (Instron 8501). The fracture surfaces were investigated with the SEM to determine the fracture mode.

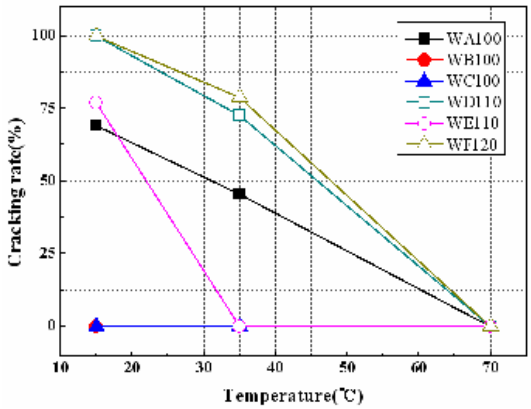

Fig. 2. The results of y-groove Tekken test.

2.5 Chemical composition and retained austenite

The qualitative chemical compositions of the microstructures of the preheating dependent specimens were estimated by using the energy dispersive spectra (EDS) found with the SEM. An X-ray diffraction (X'pert MPD 3040, Philips) technique was used to calculate the volume fraction of retained austenite, and the samples for analysis were mechanically ground and polished with 0.5 ㎛ alumina powder to give the same surface condition. The samples were scanned from 0 to 120 deg with a step size of 0.02 deg. Each step was allowed 50 s for X-ray detection.

3. Results and discussion

3.1 Y-groove Tekken test results

Fig. 2 shows the y-groove Tekken test results, with the cracking ratio plotted against the preheating temperature. As can be seen in the figure, the cracking ratio decreased with an increase in the preheating temperature. The cracking ratio of some specimens decreased to zero percent at 70℃, WB100 and WC100 show a zero percent cracking ratio even with a preheating temperature of 15℃. During decades, several forms of carbon equivalent have been proposed. But CEN (1) and CET (2) were adopted in the present discussion because these cover the major elements in the cold cracking, such as the diffusible hydrogen content, plate thickness, heat input, and yield strength of the weld metal [3, 17].

$$CEN = C + A(C) + \frac{Si}{24} + \frac{Mn}{6} + \frac{Cu}{15} + \frac{Ni}{20} + \frac{(Cr + Mo + Nb + V)}{5} + 5B$$

$$\text{where} \quad A(C) = 0.75 + 0.25\tanh\left[20(C - 0.12)\right] \tag{1}$$

$$Toin℃ = 700CET + 160\tanh(d/35) + 62HD0.35 + (53CET - 32)Q - 330$$

$$\text{where} \quad CETin\% = C + \frac{(Mn + Mo)}{10} + \frac{(Cr + Cu)}{20} + \frac{Ni}{40}. \tag{2}$$

Table 5. Volume fraction of ferrite phase and hardness of weld metal.

Identification		Preheating temperature (℃)	Volume fraction of ferrite phase (%)			Hardness (Hv5)	Cracking ratio (%)
			PF	FS	AF		
ER100S-G	WA100	15	46.0	42.0	12.0	269.0	69.2
		35	47.0	38.0	15.0	256.6	45.5
		70	31.0	11.0	60.0	251.2	0.0
	WB100	15	35.0	6.0	61.0	255.0	0.0
		35	17.0	20.0	64.0	250.3	0.0
		70	18.0	19.0	64.0	245.7	0.0
	WC100	15	29.0	12.0	60.0	273.3	0.0
		35	28.0	9.0	65.0	261.8	0.0
		70	24.0	13.0	63.0	263.2	0.0
ER110S-G	WD110	15	38.0	17.0	45.0	287.3	100.0
		35	28.0	21.0	51.0	278.0	72.7
		70	19.0	9.0	73.0	251.1	0.0
	WE110	15	37.0	20.0	45.0	278.0	76.9
		35	20.0	16.0	64.0	267.4	0.0
		70	18.0	11.0	72.0	253.5	0.0
ER120S-G	WF120	15	31.0	10.0	60.0	314.9	100.0
		35	22.0	15.0	63.0	316.0	78.8
		70	20.0	10.0	71.0	289.7	0.0

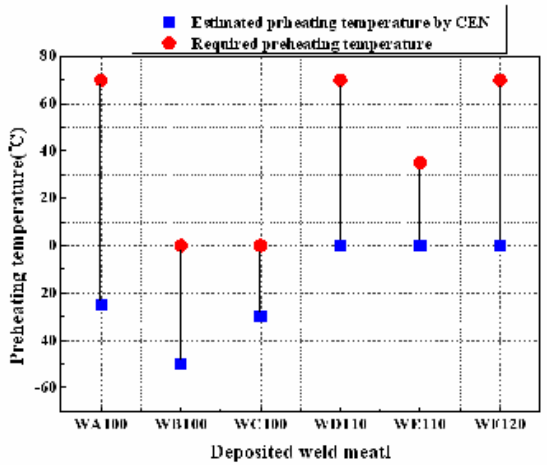

(a) Comparison between CEN and test required preheating temperature.

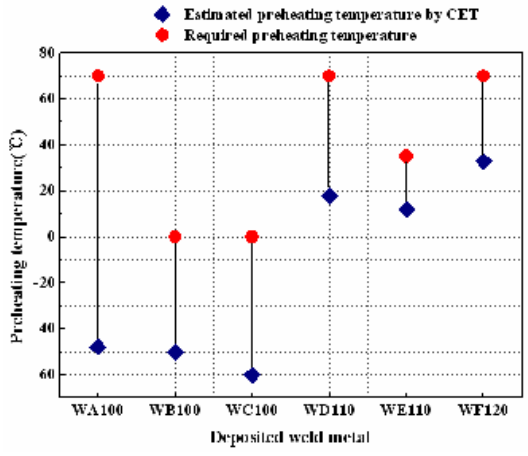

(b) Comparison between CET and test required preheating temperature

Fig. 3. Comparison of Ceq estimated preheating temperature and actual test results.

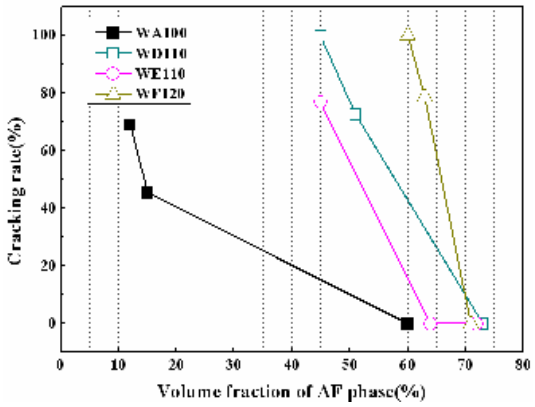

Fig. 4. Cold cracking rate as function of volume fraction of acicular ferrite.

Fig. 3 shows the mismatched values between CEN and CET for the predicted preheating temperature and actual test results. These differences prove that the carbon equivalent for the HAZ cold cracking could not predict the preheating temperature for weld metal cold cracking. However, the above two methods reflected the major factors of cold cracking. This important fact must be reflected in the international guideline for steel welding.

3.2 Results of microstructural analysis and hardness test

Based on the IIW recommendation [16], the volume fraction of the ferrite phase of each specimen was classified as PF (Polygonal ferrite), FS (Ferrite with second aligned), or AF (Acicular ferrite), as shown in Table 5. Acicular ferrite is a well known microstructure that improves the toughness of the weld metal and the resistance to cold cracking. The results of the present study also show that increasing the volume frac-

Table 6. Estimated chemical composition of y-groove Tekken test specimens (wt%) and prior austenite grain boundary size (㎛).

Identification		Preheating temperature (℃)	Si	Mn	Ni	Cr	Al	Ti	V	Fe	Prior austenite GB size (㎛)
ER100S	WA100	15	0.36	1.69	-	-	-	-	-	Balanced	3.9
		35	0.74	1.65	-	-	-	-	-	Balanced	3.9
		70	0.35	1.99	-	-	0.65	1.02	0.22	Balanced	7.8
	WB100	15	0.35	1.16	-	-	-	-	-	Balanced	5.5
		35	0.43	1.82	-	-	-	-	-	Balanced	5.5
		70	0.39	1.46	-	-	-	-	-	Balanced	7.8
	WC100	15	0.54	1.29	1.58	0.59	-	-	-	Balanced	5.5
		35	0.61	1.36	1.44	0.57	-	-	-	Balanced	5.5
		70	0.40	1.48	1.59	0.83	-	-	-	Balanced	5.5
ER110S	WD110	15	0.57	1.67	-	-	-	-	-	Balanced	5.5
		35	0.48	1.47	-	-	-	-	-	Balanced	7.8
		70	-	1.82	-	-	-	-	-	Balanced	7.8
	WE110	15	0.56	1.47	-	-	-	-	-	Balanced	5.5
		35	0.48	2.03	-	-	-	-	-	Balanced	5.5
		70	-	1.82	-	-	-	-	-	Balanced	7.8
ER120S	WF120	15	-	2.32	-	-	-	-	-	Balanced	5.5
		35	-	2.05	-	-	-	-	-	Balanced	5.5
		70	-	2.05	-	-	-	-	-	Balanced	7.8

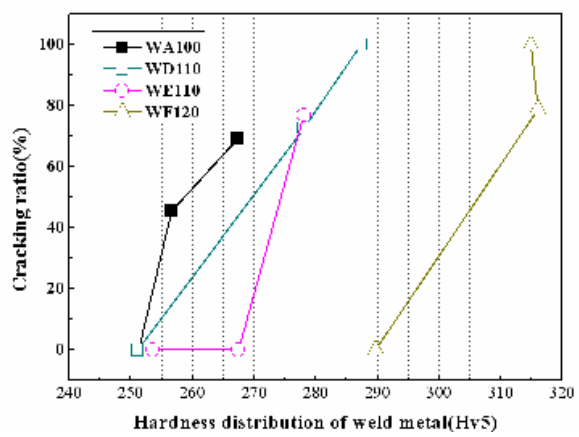

Fig. 5. Cold cracking rate as function of weld metal hardness.

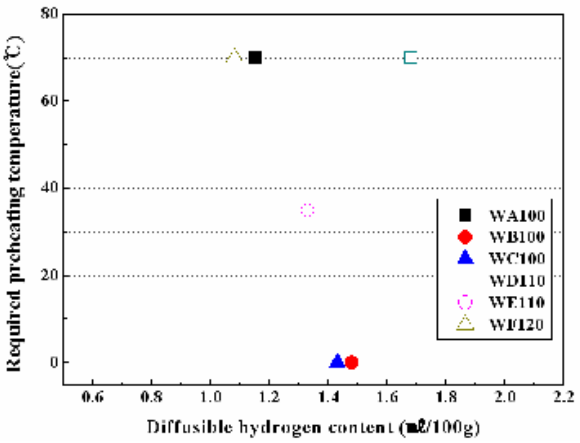

Fig. 6. Required minimum preheating temperature as function of diffusible hydrogen content.

tion of acicular ferrite dramatically decreased the cracking ratio. Fig. 4 shows the cracking rate of each weld as a function of the acicular ferrite volume fraction. The acicular ferrite was definitely the most dominant microstructure that could prevent cold cracking in the weld metal.

The average hardness value (Hv5) is shown in Table 5. The results show that with an increase in the preheating temperature, the weld metal hardness decreased gradually due to the low cooling rate and the cracking ratio also decreased. Fig. 6 plots the required minimum preheating temperature from the y-groove Tekken test results as a function of the diffusible hydrogen content. However, a specific correlation between the hydrogen level and preheating temperature was not found.

3.3 The chemical composition and austenite grain size

Table 6 gives the chemical composition estimated by EDS, along with the prior austenite grain size. TiO, TiN, Al_2O_3, and VN promote the formation of acicular ferrite, acting as point sites from which intragranular nucleation is developed [7-9]. The data for oxygen, carbon, nitrogen, and boron are not presented in the present study because elements with atomic numbers lower than nine were not detectable with the EDS.

It is interesting that, among the WA100 welds, Ti, Al, and V were only found in the specimen with the preheating condition of 70℃. The Ti, Al, and V depletion may be explained by saying that these acicular ferrite promoting elements acted to form the acicular ferrite and so were depleted in the welds [18]. Fig. 7 shows evidence in the form of angular inclusions in the WB100 weld with the 15℃ preheating temperature. Kluken et al. reported that the sequence of inclusion formation in Al-Ti-Si-Mn deoxidized steel weld metals can be outlined as follows [19]. VN could be placed between Al and Ti; thus,

Table 7. Melting temperatures of selected acicular ferrite nucleating inclusions [12, 18].

Compound	Melting temperature (℃)	Reference
Al_2O_3 (Corundum)	2050	[12]
VN	2050	[18]
3 Al_2O_3 · SiO_2 (Mullite)	1850	[12]
TiO	approximately 1800	
SiO_2 (β -Cristobalite)	1723	
Al_2O_3 · MnO (Galaxite)	approximately 1620	
MnS	1620	
Mn_3O_4	1560	
2MnO · SiO_2 (Tephroite)	1345	
3MnO · Al_2O_3 · 3 SiO_2 (Spessartite)	1195	

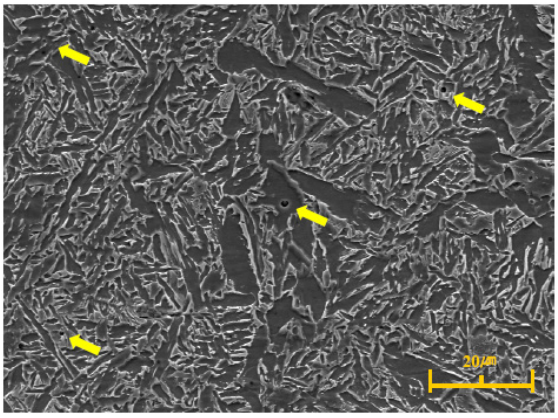

Fig. 7. Angular inclusions of WB100 weld of 15℃ preheating temperature.

the sequence of inclusion formation might be Al-V-Ti-Si-Mn, as shown in Table 7, the melting temperatures of selected oxidizes and nitrides [7, 20].

The depletion of acicular ferrite promoting elements, Ti, Al, and V in the WB100 weld with the 70℃ preheating temperature can be explained that those in welds with a preheating temperature of 70℃ could nucleate it because of the relatively large austenite grain size and the longer retention time as Dallam et al. reported [10]; while, the acicular ferrite promoting elements in welds with a preheating temperature of 15℃ and 35℃ could not nucleate the acicular ferrite phase because of a relatively small austenite grain size. Fig. 8 shows how, due to the relatively small austenite grain size, second phase ferrite and polygonal ferrite developed in the WA100 weld with a 15℃ preheating temperature. It is concluded that the austenite grain size is important in determining the proportions of the various transformation products.

It can also be explained that in the case of the small austenite grain size in the specimens with the preheating temperatures of 15℃ and 35℃, there was not enough space for

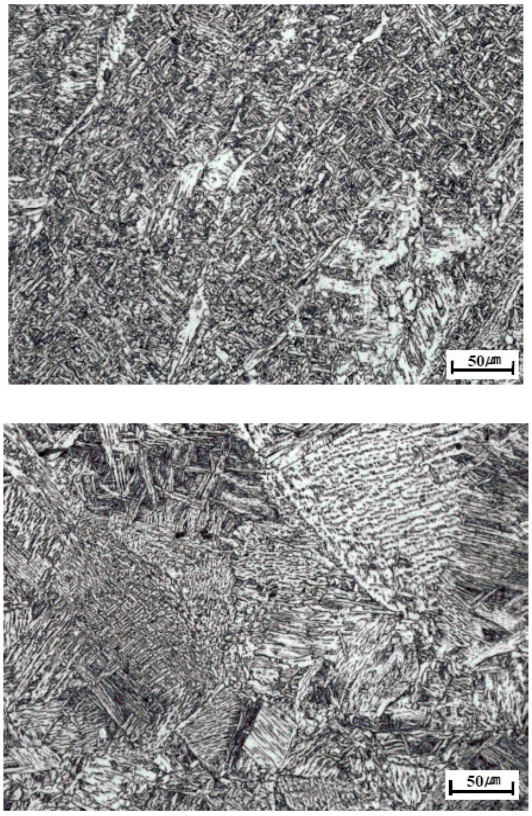

Fig. 8. Polygonal ferrite and ferrite with second phase developed in the WA100 weld of 15℃ preheating temperature.

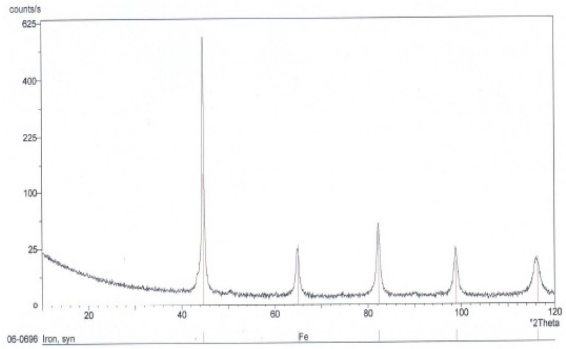

(a) WA100 weld of 15℃ preheating temperature

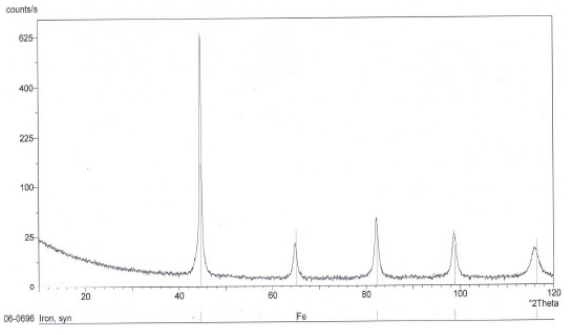

(b) WA100 weld of 70℃ preheating temperature

Fig. 9. X-ray analysis of WA100 welds which contain 0 volume % retained austenote.

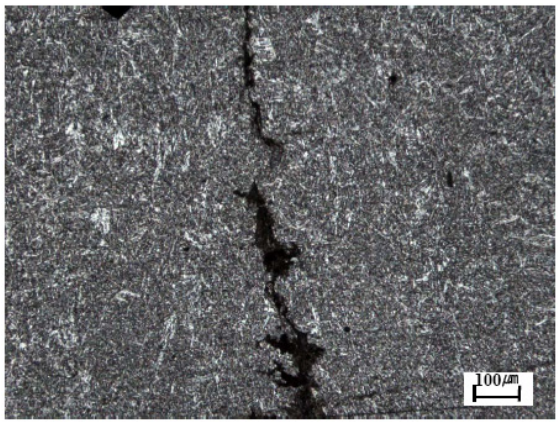

Fig. 10. Micrograph showing the clod cracking.

developing the acicular ferrite and the driving force for nucleating due to the relatively shorter retention time. Because second phase ferrite and polygonal ferrite forms at temperatures higher than acicular ferrite, the acicular ferrite transformation might be affected by either the second phase ferrite or polygonal ferrite [10]. The decomposition of austenite is a competitive process between polygonal ferrite and internally nucleated transformation.

3.4 The retained austenite

Fig. 9 shows an X-ray diffraction analysis of the WA100 welds, with no retained austenite revealed. The zero volume percent of retained austenite is thought to be the result of the relatively faster thermal cooling rate, which did not allow the time needed to form the retained austenite in the present study. Furthermore, Park et al. reported that a liquid-nitrogen-quenched HSLA weld deposit sample had almost zero volume percent of retained austenite. Even though a certain amount of retained austenite is inevitable in HSLA steel weld deposits because of the thermal cooling cycles of welding [11], at a low preheating temperature ($\leq$100℃) and low heat input ($\leq$1.5 KJ/㎜), no retained austenite was found. Therefore, its role as a hydrogen trapping site had no effect on the cold cracking susceptibility.

3.5 Cracking propagation path and fracture surface

Metallographic examinations were conducted on the y-groove Tekken specimens and the results are shown in Figs. 10 and 11. Fig. 10 shows the cold cracking that was developed in the WF120 welds. This crack appears to propagate through the columnar grains at the early stage of propagation, but the propagation route was found to be different when the crack propagated through the acicular ferrite. It can be seen that the crack followed the grain boundaries of the columnar grains at an early stage, but when it propagated through the fine acicular ferrite, it was blunted and propagated to different paths. Fig. 11(a) shows how the crack appears to be blunted intermittently during its

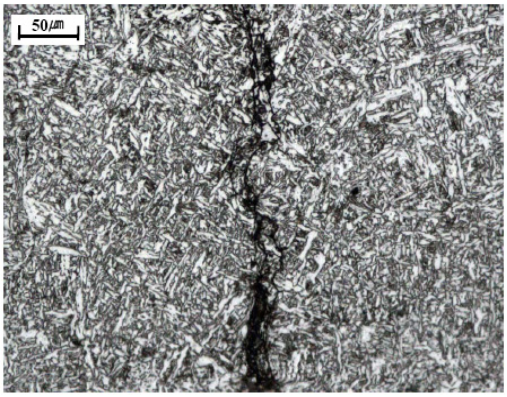

(a) Optical micrograph

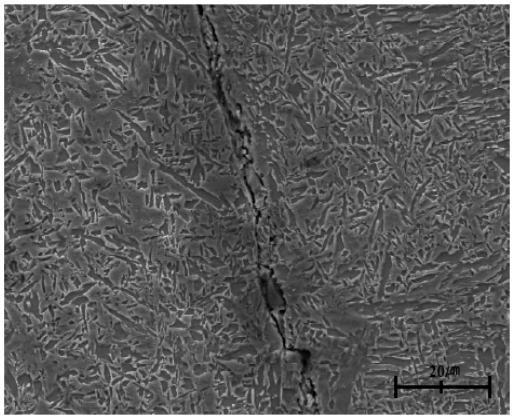

(b) SEM micrograph

Fig. 11. Micrograph illustrating the branching and blunted crack.

propagation across the acicular ferrite, along with the branching cracks that developed immediately after blunting. These phenomena are also observed in the SEM image of Figs. 8(b). Such cracking behavior is believed to be the result of the fine interlocking nature of the acicular ferrite microstructures [3].

After metallographic examinations, the cracked specimens were opened and examined under SEM. Fig. 12(a) shows a quasi-cleavage fracture in the WA100 weld, while (b) shows the quasi-cleavage fractures of early crack growth in WD110, WE110, and WF120. Fig. 12(c) shows the intragranular fractures of late crack growth in WD110, WE110, and WF120.

It is clear that these cracks developed mainly in an intragranular fracture mode along the columnar grain boundaries, and it was found that small micro cracks could be situated in either grain boundary ferrite or intragranular microstructures, as shown in Fig. 9 and that, at least for 270 Hv5, the crack path was not preferentially located in grain boundary ferrite [21, 22].

4. Conclusions

The effects of the microstructural constituents, chemical compositions, and retained austenite on high-strength weld metal were investigated using a y-groove Tekken test with

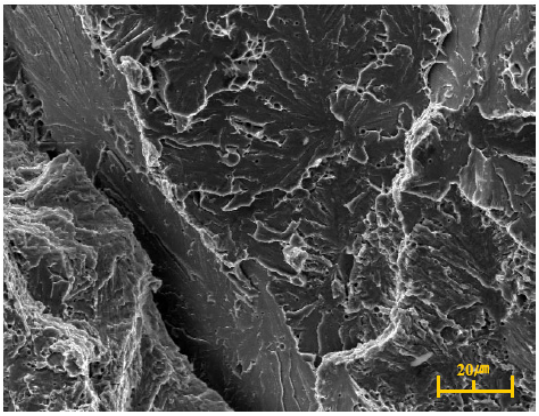

(a) Quasi-cleavage fracture

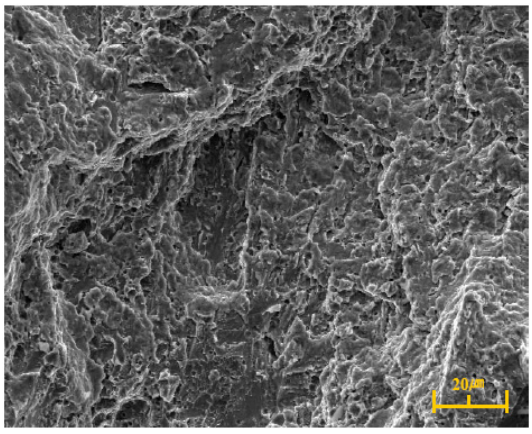

(b) Quasi-cleavage fracture at early crack growth stage

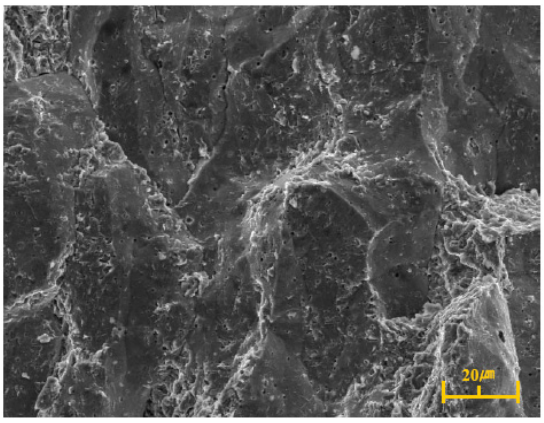

(c) Intragranular fracture at late crack growth stage

Fig. 12. Clod cracking fracture surface.

three different preheating temperatures (15℃, 35℃, and 70℃) and the major results are summarized as follows:

(1) Increasing the volume fraction of acicular ferrite improved the resistance to cold cracking in weld metal, and the microstructural characteristics of the deposit appeared to be more important than hardness and diffusible hydrogen content in low hydrogen level weld metal.

(2) When a crack was propagated through fine acicular ferrite, the crack blunted and branched to different paths because of the fine interlocking nature of the acicular ferrite microstructures.

(3) To nucleate acicular ferrite by the inclusion of the Ti, Al, and V elements, proper austenite grain size and retention time were required, and the sequence of inclusion formation could be suggested to be as follows: Al-V-Ti-Si-Mn.

(4) In the weld metal with a low preheating temperature ($\leq$100℃) and low heat input ($\leq$1.5 KJ/㎜), no retained austenite was found and it had no effect on the cold cracking.

Acknowledgement

This work was supported for two years by Pusan National University Research Grant.

References

[1] S. Kou, *Welding metallurgy*, John Wiley and Sons, New York, 1987.
[2] N. Yurioka, *ISIJ Int.*, 6 (2001) 566-570.
[3] N. Yurioka, T. Kasuya, *Weld in the World*, 5 (1995) 31-38.
[4] T. Kitada, K. Fukuda, *Nippon Kokan Technical Report*, Overseas, 47 (1986).
[5] J. W. Fisher, R. J. Dexter, *Weld J.*, 35 (1994).
[6] J. H. Kim, J. S. Seo, H. J. Kim, H. S. Ryoo, K. H. Kim and M. Y. Huh, *Metals Mater. Int.*, 14 (2008) 239-245.
[7] J. M. Dowling, J. M. Corbett and H. W. Kerr, *Metall. Trans. A*, 17A (1986) 1611-1623.
[8] I. Madariaga, J. L. Romeo and I. Gutierrez, *Metall. Mater. Trans. A*, 29A (1998) 1003-1015.
[9] F. Ishikawa, T. Takahashi and T. Ochi, *Metall. Mater. Trans. A,* 25A (1994) 929-936.
[10] C. B. Dallam and D. L. Olson, *Weld. J.*, (1989) 198s-205s.
[11] Y. D. Park, I. S. Maroef, A. Landau and D. L. Olsen, *Weld. J.*, (2002) 27s-35s.
[12] C. R. Wildash, C. Cochrane, R. Gee and D. J. Widgery, *Trends in weld. Res.*, Int. Conf., 745-750.
[13] AWS A 4.3, American Welding Society, (1993).
[14] AWTM A 370, ASTM International, (2010).
[15] AWS D 1.1, American Welding Society, (2001).
[16] D. J. Abson and E. R. Dolby, IIW Doc. IXJ-29-80 (Dolby) (1980).
[17] D. Uwer and H. Hohne, IIW Doc. IX-1631-91 (1991) 282-286.
[18] J. M. Gregg and H. K. D. H. Bhadeshia, *Metall. Mater. Trans. A*, 25A (1994) 1603-1611.
[19] A. O. Kluken and O. Grong, *Metall. Trans. A*, 20A (1989) 1335-1349.
[20] Y. I. Matrosov and V. N. Anashenko, *Metal Sci. And Heat Treat.*, 10 (1971) 78-80.

[21] P. H. M. Hart, *Weld. J.* (1986) 14s-22s.
[22] H. J. Kim and B. Y. Kang, *ISIJ Int.*, 5 (2003) 706-713.

Hui-Jun Yi received his M.S. degree from Graduate School of Pusan National University, Korea. He is currently in the doctoral course of Graduate School of Pusan National University, Korea. Mr. Yi's research interests include weldability of ferrous and nonferrous metals and CAE for predicting welding residual stress and distortion.

Yong-Jun Lee received his M.S. degree from Graduate School of Pusan National University, Korea. He is currently in the doctoral course of the Graduate School of Pusan National University, Korea. Mr. Lee's research interests include laser welding and CAE for predicting fatigue life.

Jong-Yun Kim received his B.S. in Mechanical Engineering from Pusan National University, Korea. He is currently in the master's course of the Graduate School of Pusan National University, Korea. Mr. Kim's research interests include friction stir welding and fatigue life of stainless steel weldment.

Sung-Su Kang received his M.S. and Ph.D. degrees from Graduate School of Seoul National University, Korea. He is currently a Professor at the School of Mechanical University at Pusan National University in Pusan, Korea. Dr. Kang's research interests include plastic working process and CAE for plastic working.